AP Positioning Strategies for Deploying a UAV-Enabled Network: Modeling and Simulation

Guido Betcher-Sbrolla
Dept. Networks Engineering
Universitat Politècnica de Catalunya
Barcelona, Spain
guido.betcher@upc.edu

Eduard Garcia-Villegas
Dept. Networks Engineering
Universitat Politècnica de Catalunya
Barcelona, Spain
eduardo.garcia@upc.edu

Elena Lopez-Aguilera
Dept. Networks Engineering
Universitat Politècnica de Catalunya
Barcelona, Spain
elena.lopez@upc.edu

***Abstract*—Flying Ad-hoc Networks (FANETs) offer a versatile solution for extending connectivity to ground stations (STAs). However, optimizing the deployment of Flying Access Points (F-APs) remains a challenge, particularly under diverse mobility conditions. This paper proposes and evaluates several F-AP deployment strategies for mobile ground users across distinct mobility models. As a key contribution, it establishes criteria for selecting the optimal positioning strategy based on STA movement characteristics. We compare three approaches: (i) static positioning, which serves as a benchmark where the Wi-Fi Access Point (AP) remains fixed, (ii) dynamic positioning at the centroid of the STA locations; and (iii) dynamic positioning based on optimizing different network performance metrics. These strategies are assessed via simulations and analytical modeling using various Key Performance Indicators (KPIs). Results indicate that static positioning is ineffective under non-homogeneous STA distributions. Conversely, the centroid-based strategy provides performance comparable to the one optimizing the aggregate throughput at the F-AP with significantly lower computational overhead and power consumption. The dynamic strategy that maximizes the aggregate throughput at the GCS demonstrated good performance in all scenarios. Even for those where the STAs move in clusters, a scenario where the rest of the strategies had worse results. These findings offer critical insights for deploying Wi-Fi coverage in dynamic environments, such as search and rescue missions.**

***Index Terms*—Flying-AP, network optimization, Wi-Fi, UAV, UAV-based network, FANET, modeling**

I. Introduction

Unmanned Aerial Vehicle (UAV) applications for Flying Ad-hoc Network (FANET) deployments attract significant research interest due to their high mobility, versatility, and rapid deployability, which enable new possibilities across a wide range of applications. This network typology is often proposed for post-disaster or rural scenarios where there is no Internet connectivity due to the infrastructure being damaged or absent [1, 2]. In this context, its function is to provide Internet access to ground user stations (STA). This service is deployed by means of an access network and, depending on the architecture, also a backhaul network. The access network is composed of a UAV with the role of Access Point (AP), also called Flying Access Point (F-AP); on the other hand, the backhaul network consists of the link between the F-AP and the node with the role of gateway (GW), which provides Internet access. Choosing the position in which the F-AP is deployed is a complex task, and this paper attempts to find solutions to this problem. The GW can be a Ground Control Station (GCS), another UAV, or the UAV with the F-AP role itself. For the last two cases, the GW also receives the name of Flying Gateway (F-GW). The most common approach to connect the GW to the Internet is with cellular (e.g., 4G or 5G) or satellite links. However, optical fiber is also proposed in some studies [3, 4].

This article proposes several strategies to deploy an F-AP that provides Wi-Fi connection to a set of mobile ground users. It is assumed that STA coordinates are known since they can be estimated using different techniques, for example, based on Angle of Arrival (AOA) and Time of Arrival (TOA) measurements [5, 6]. The network architecture is defined by a variable number of STAs, an F-AP, and a GCS that acts as a GW, as shown in Fig. 1.

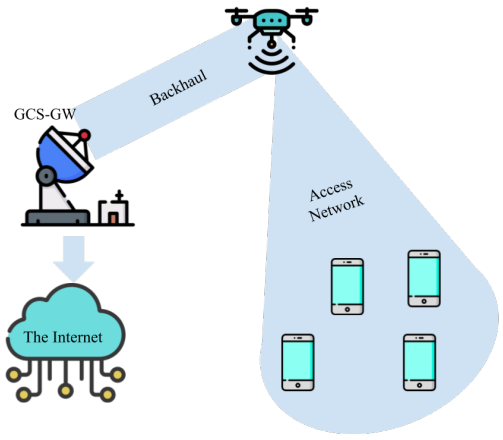


Fig. 1. Scenario architecture.

Both the access network (STA–F-AP) and the backhaul link (F-AP–GW) leverage Wi-Fi 7, selected for its wide support in unlicensed bands and high-capacity capabilities. We consider that the F-AP carries two Wi-Fi 7 devices, one for the access network deployment and the other to establish the backhaul link with the GCS. Both devices operate at different frequency channels in the 5 GHz band, allowing them to transmit and receive simultaneously without interfering with each other. Three F-AP placement strategies are evaluated: (i)

979-8-3195-0167-7/26/$31.00 ©2026 IEEE

static (benchmark), (ii) dynamic geometric-based placement at the STA locations' centroid, and (iii) metric-optimized dynamic placement. These are assessed via simulation and analytical modeling using various Key Performance Indicators (KPIs) and mobility models. The current literature often lacks diverse mobility testing, typically focusing on static or limited dynamic scenarios. Conversely, we evaluate our strategies across distinct mobility patterns to identify the most suitable approach based on specific user behavior, representing the primary contribution of the paper.

The structure of the article is as follows. Sec. II presents a survey of the consulted literature to build the state of the art. Sec. III describes the proposed strategies to place the F-AP. In Sec. IV, the model used to simulate the network and the performance of the proposed strategies are analyzed. To evaluate the strategies, three different mobility models are tested to characterize the movement of the STAs. Finally, Sec. V presents the conclusions and future work.

II. Related Work

Researchers have analyzed Wi-Fi AP placement optimization since the birth of this technology [7]. As robotics developed, researchers began to propose the deployment of mobile APs [8, 9]. Nakata et al. implement mechanisms based on the power received by a mobile robotic AP to optimize its position in [9]. Al-Hourani et al. [10] pioneered the altitude optimization for UAV-based AP deployment by incorporating the air-to-ground propagation model for urban environments. However, the authors do not address the placement optimization in the horizontal plane (i.e., x, y coordinates). In [11], a multi-UAV 3D placement strategy is presented for the first time. This strategy maximizes the coverage area given a predefined number of UAVs without overlapping their coverage zones. Although the coverage area is maximized, it does not ensure connectivity for all users.

In more recent studies, there has been an increase in the variety of problem formulations and strategies applied to solve the problem. The channel allocation problem was considered in [12]. There, the problem is divided into two subproblems. Channel allocation and capacity-based placement subproblems are solved alternately over time, so the UAV tends towards a stable solution. To solve the problem of F-GW positioning to provide Internet access to several F-APs [13] proposes the Fast Gateway Placement (F-GWP) algorithm. This algorithm first selects a Modulation and Coding Scheme (MCS) that ensures connectivity between all F-APs and the F-GW. Then the transmission power of the nodes is reduced until the coverage areas of all F-APs overlap at a single point. This point is selected as the optimal position for the F-GW. Papanikolaou et al. [14] propose a Graph Neural Network trained on NS-3-generated datasets to solve the F-AP positioning problem. Nevertheless, many of these solutions neither ensure deployment in globally optimal locations nor address objectives beyond coverage optimization. To address this gap, this paper proposes a deployment strategy that performs a comprehensive search for optimal placement of UAVs. This strategy takes into account key network metrics, including aggregate throughput measured in the F-AP and in the GW. It also tries to decipher the advantages and disadvantages of optimization-based strategies versus heuristics.

In [15], the authors also propose a mechanism based on Exhaustive Search (ES) to optimize the position of the Wi-Fi F-AP. Network optimization is achieved by minimizing the number of UAVs deployed and the energy consumption related to the communications of STA devices. In our work, a state-of-the-art Wi-Fi standard (i.e., Wi-Fi 7) is adopted. Furthermore, we leverage the 5 GHz band to exploit its higher transmission power and consequently extend the coverage range. Moreover, unlike the existing literature, this paper introduces dynamic positioning mechanisms, which are evaluated in various mobility models. This analysis enables the identification of preferable placement strategies under specific mobility patterns and assesses how the algorithmic approach (whether geometric or optimization-based) impacts energy consumption.

III. Proposed strategies

All strategies are evaluated under the same scenario, defined as a square area with 167-meter sides. This size is chosen to simplify the analysis by avoiding hidden-node effects. Therefore, the diagonal of the region matches the maximum communication range achieved in our field measurements (236 meters, as shown in Fig, 2). This ensures that all STAs remain within mutual carrier-sensing distance. In practice, hidden-node issues can be alleviated through legacy mechanisms such as RTS/CTS, as well as through modern techniques such as OFDMA, MU-MIMO, and beamforming. The STAs move inside this region at a height of 1.5 meters. The GCS-GW is also placed inside this region at 1.5 meters high, but remains in the same position throughout the mission. The F-AP is located within a two-dimensional plane at 20 meters high, assuming unobstructed paths to all STAs. Its (x, y) coordinates are determined following several strategies. The strategies proposed in this paper are divided into two main categories: static and dynamic strategies. Static strategies deploy an F-AP at a fixed position, while in dynamic positioning strategies, the F-AP position is updated every Δt time interval. The UAV maximum speed is fixed to 5 m/s. Table I summarizes the values of all configuration parameters defined throughout the paper.

A. Static AP over GCS location

In this case, the F-AP is deployed directly above the GCS. This strategy is used as a benchmark and allows evaluating the potential improvements of having an F-AP that adapts its position as the STAs move.

B. Centroid-based dynamic strategy

The first dynamic placement strategy uses geometric criteria, placing the F-AP at the centroid of the STA positions. Thus, for a scenario with *N* STAs, the target position is given by Eq. 1.

$$(x, y) = \frac{1}{N}\left(\sum_{i=1}^{N} x_i, \sum_{i=1}^{N} y_i\right) \tag{1}$$

TABLE I
SIMULATION PARAMETERS CONFIGURATION.

Parameter		Value
GCS location	Mobility Model 1	center
	Mobility Model 2	bottom-left
	Mobility Model 3	center
Region size $[m]$		167×167
Simulation duration $[s]$		240
Time interval (Δt) $[s]$		1
Height of STAs $[m]$		1.5
Altitude of UAV $[m]$		20
STAs max. speed $[m/s]$		2
UAV max. speed $[m/s]$		5
Number of STAs (N)		5 , 10 & 15
ES resolution $[m]$		1
Air density (ρ) $[kg/m^3]$		1.225
Reference UAV		DJI Phantom
UAV mass $[kg]$		1.38
UAV rotors speed $[rpm]$		5300

This strategy minimizes the average distance between STAs and the F-AP. Assuming similar obstruction conditions and transmit powers from all STAs, shorter distances directly translate to higher MCS levels, which in turn improves capacity-related metrics.

C. Model-based dynamic strategies

The second dynamic placement strategy involves conducting an ES to determine the optimal position considering a particular network metric. This means dividing the region of interest into a grid and measuring the target metric for each position. The position with the most favorable value is then selected. If multiple positions offer the optimal value, the one closest to the F-AP's current position is chosen. The grid resolution was set to 1 meter with updates every $\Delta t = 1s$. The ES is used here to provide an upper-bound reference for the evaluated KPIs and to support a controlled comparison between placement strategies. Nevertheless, although computationally demanding, this approach remains practical for the considered scenarios with 5–15 STAs, with further details on its complexity provided in Sec. IV-C2. In operational deployments, lower-complexity heuristics would be preferable and are expected to achieve similar performance with only a limited KPI penalty. The metrics evaluated are the aggregate throughput at the F-AP (i.e., access network capacity) and the aggregate throughput at the GCS (i.e., Internet access capacity). Each metric and its derivation are detailed below.

1) Maximize aggregate throughput at the AP (MAT-A): This metric measures the transmitted data rate at the application level from the STAs to the F-AP when the STAs transmit at full buffer (i.e., in saturation). An analytical model has been used to calculate this metric. This model allows estimating the aggregate throughput at the F-AP knowing the individual capacity of each link between F-AP and STA.

This model is based on Eq. 2, derived from the expression provided in [16]. In Eq. 2, the individual link capacities (r_i) are used to compute the aggregate throughput (S_{AP}). Empirical measurements were conducted using commercially available Wi-Fi 7 devices to generate a throughput vs. distance table used to estimate the capacities of individual links in real scenarios. The procedure involved measuring the achievable throughput at multiple separation distances. The measurement setup consisted of a PC connected to an AP using 10 Gbps Ethernet and a mobile device (i.e., STA) connected to the same AP using Wi-Fi 7. The devices used were Huawei AirEngine 8771-X1T and Xiaomi 13T Pro for the AP and STA, respectively. The link configuration was done to maximize the AP's coverage range. The AP was configured in the 5 GHz band. The measurements were taken using the iPerf application with the server running on the PC and the STA acting as the client (i.e., up-link measurements). The measurements were conducted outdoors at the UPC Campus del Baix Llobregat in Castelldefels. The experimental setup comprised 28 distinct positions ranging from 1 to 235 m from the AP, all of which met line-of-sight (LoS) conditions. A higher spatial resolution was adopted at shorter distances to accurately capture the MCS transitions. For each location, ten different measurements were recorded. Fig. 2 presents the resulting throughput–distance curve, where each marker represents the average throughput obtained from the ten different measurements.

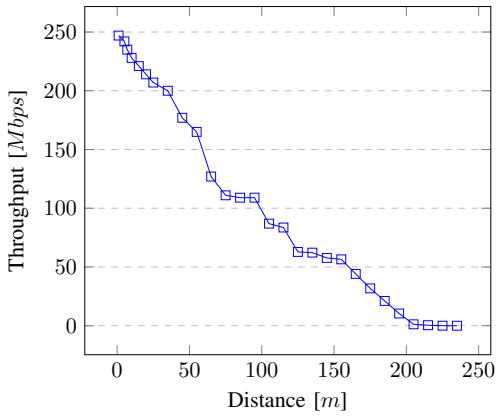


Fig. 2. Link capacity measurements for 20 MHz channel at 5 GHz band.

For distances between two measurements, the values were interpolated. Therefore, the first step is to compute the distance between the STA and the F-AP, and then the corresponding throughput value from the throughput vs. distance table is assigned. Since the model is grounded in empirical measurements, it inherently captures real-world communication phenomena such as interference, contention, retransmissions, channel variability, and MCS adaptation. Consequently, these factors are directly factored into the capacity estimation of individual links. Once the throughput of all the links in the network has been obtained, Eq. 2 is applied to provide the aggregate throughput.

$$S_{AP} = \frac{1}{\sum_{i=0}^{N} \frac{1}{r_i}} \tag{2}$$

2) Maximize aggregate throughput at the GCS (MAT-G): To calculate the aggregate throughput at the GCS-GW, both the

access network and the backhaul link between the F-AP and the GCS are considered. The calculation is as follows. First, the aggregate throughput at the F-AP S_{AP} is computed as described in the previous subsection. Second, the capacity of the link between the F-AP and the GCS (S_{BH}) is obtained by finding the throughput value for the distance between the F-AP and GCS in the throughput vs. distance table (cf. Fig. 2). Finally, since both networks operate on independent channels, there is no operational interdependence between them, meaning they function as entirely independent networks. Consequently, the network with the lower aggregate throughput capacity (either the access or the backhaul network) constitutes the bottleneck for traffic traveling from the STAs to the GCS-GW. Therefore, the aggregate throughput at the GCS is calculated as:

$$S_{GCS} = \min(S_{BH}, S_{AP})$$

IV. Performance analysis

This section first validates the accuracy of the throughput models for the evaluated scenarios. Following validation, the proposed strategies are evaluated under various STA mobility models.

A. Model validation

In [17], a similar model to the one used in this paper is validated for calculating the capacity of multi-hop networks. This subsection analyzes whether the model used in this paper is also valid for the proposed scenarios. The main differences are that the STAs are not positioned along a straight line, but randomly within the scenario; and, instead of only point-to-point multi-path transmissions, this case considers two-hop paths: first, point-to-multi-point up-link transmissions (STAs to F-AP), followed by a point-to-point link from F-AP to GCS-GW.

To validate the throughput models presented in Sec. III, we used NS-3 to simulate the target scenarios and obtain aggregate throughput at the F-AP values for all candidate F-AP positions. We then compared the optimal position identified through simulation, considered our ground truth, with the one predicted by the models in Sec. III-C. The scenario was sampled with an evenly spaced $i \times j$ grid to generate candidate F-AP locations.

In NS-3, the STAs are implemented as UDP clients, and the F-AP and the GCS-GW implement UDP servers to measure S_{AP} and S_{GCS}, respectively (cf. Sec. III-C). The F-AP node shares a wireless local area network (WLAN) with the STA nodes, while the GCS node forms a separate WLAN with the F-AP. Therefore, the F-AP has two Wi-Fi interfaces. During the NS-3 simulation, the STA nodes first generate traffic to the F-AP for 10 seconds. After 10 seconds, the traffic stops and the UDP server running on the F-AP is disabled. After 5 seconds, necessary for network decongestion, traffic is generated again from the STAs, this time with the GCS address as the destination.

Once all F-AP positions have been evaluated, those maximizing aggregate capacities according to the model (towards F-AP and GCS) are selected. We then compare the S_{AP} and S_{GCS} values reported by NS-3 at the model-selected positions against the global maximums. Fig. 3 shows the aggregate throughput at the F-AP in every grid position for a particular STA distribution. It shows the resulting values using both the analytical model and NS-3 simulations.

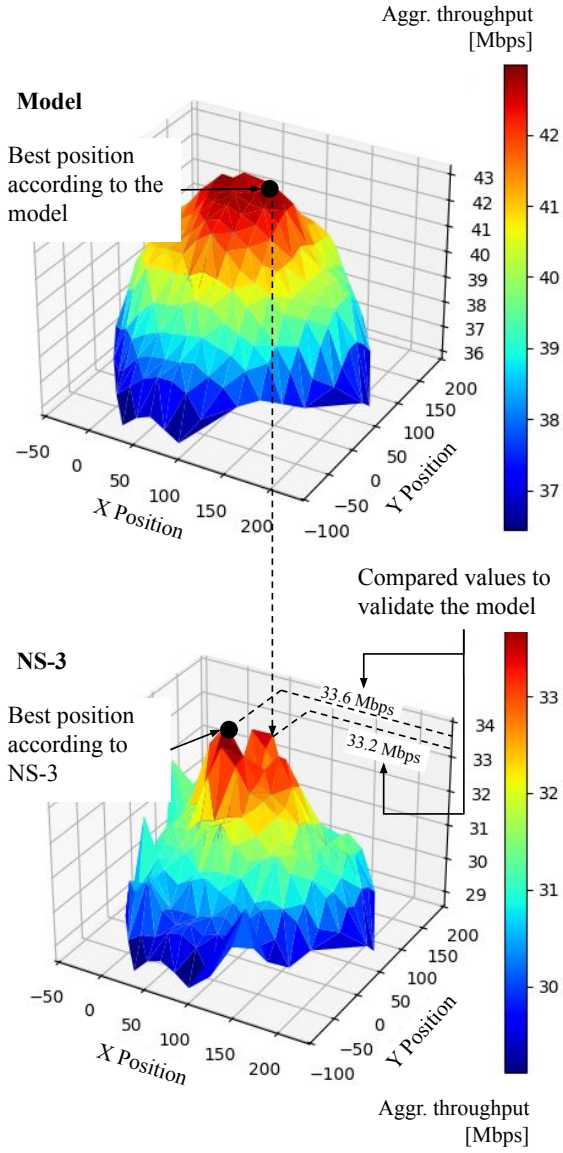


Fig. 3. Example of access network aggregate throughput depending on F-AP position.

This process was carried out with scenarios from 5 to 50 STAs. For each number of STAs, 10 random droppings were simulated. Fig. 4 shows the mean relative error between the aggregate throughput reported by NS-3 in the global maximums and in the model-selected positions. The mean relative error is calculated for different number of STAs from 5 to 50. In the case of aggregate throughput at the GCS, the average error is 0.90%, while the difference for the aggregate throughput at the F-AP is 0.74%. Given relative errors near 1%, the proposed models effectively identify near-optimal F-AP positions at lower computational cost.

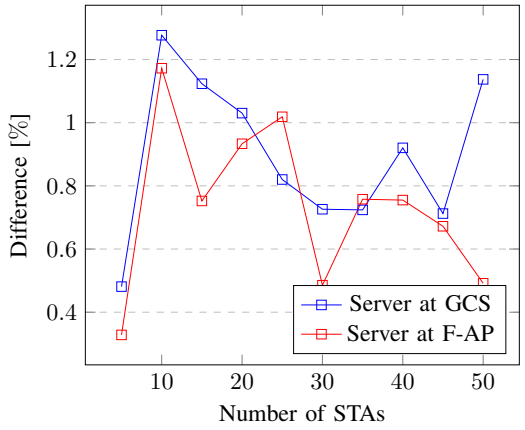


Fig. 4. Difference in NS-3 aggregate throughput between the best position based on the model and the best position based on NS-3.

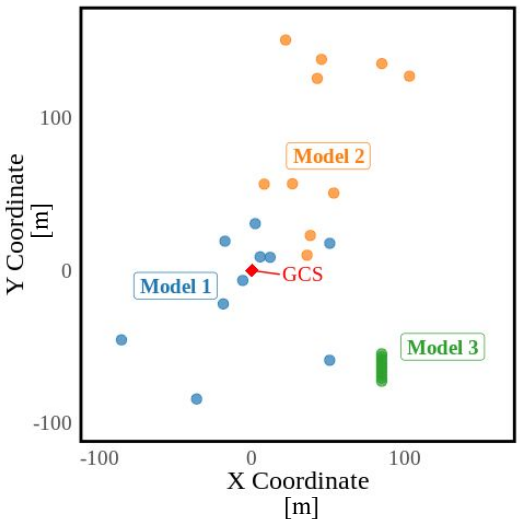


Fig. 5. Example of STA positions after 2 minutes of simulation for three different mobility models.

B. Strategies evaluation

To evaluate the performance of the different strategies discussed in Sec. III, three scenarios have been designed in which the STAs move following different mobility patterns. For each scenario, an evaluation is performed with 5, 10, and 15 STAs. All STAs move at a randomly chosen speed between 1 and 2.5 m/s, corresponding to common walking speeds. When any STA is at the edge of the mission area, the velocity component(s) pointing away from the map are reversed. The F-AP is assigned a maximum speed of 5 m/s, which is a typical speed for a rotor UAV. Fig. 5 shows the position of the STAs after 2 minutes of simulation.

1) Mobility model 1: The initial position for STAs, F-AP, and GCS corresponds to the center of the square delimiting the mission region. The STAs follow a random mobility pattern leaving from the center of the region (Tab. I). The STAs choose a totally random direction and move forward for 5 Δt intervals before changing the direction randomly again.

With this mobility pattern, STA positions become uniformly distributed in the long run, so the F-AP positions that maximize throughput tend to lie near the center. Along the simulation shown in Fig. 6, all strategies maintain similar F-AP positions for the first 150 seconds. This is reflected in the fact that the KPI values are very similar across all strategies (Fig. 6 and 7). From then on, the difference between static and dynamic strategies starts to increase in all KPIs. Even so, dynamic strategies only manage to improve the average aggregate throughput during the entire mission by 1% compared to the static strategy (Table II). When comparing dynamic strategies between them, there are no relevant differences. The same happens when comparing the aggregate throughput at the F-AP and at the GCS. For this reason, the dashed lines in Fig. 6 are not visible. Under uniform STA distribution and with a short backhaul link whose capacity exceeds that of the access network, all dynamic strategies offer equivalent performance.

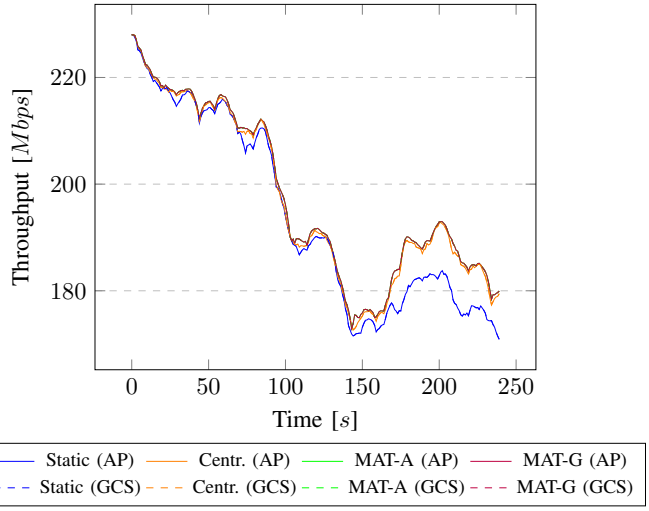


Fig. 6. Aggregated throughput to F-AP (solid line) and GCS (dashed line) for each F-AP positioning strategy in a scenario where STAs follow mobility pattern 1.

2) Mobility model 2: The initial positions of STAs, F-AP, and GCS are located in the lower-left corner of the evaluation area (Tab. I). The STAs move with a constraint on their turning angle. At the beginning of the simulation, all STAs select a random initial direction. After moving forward for 5 Δt intervals, each STA changes its trajectory by a random angle between -45° and 45°. STAs then continue moving forward for 5 Δt intervals more, repeating this process iteratively.

In this case, since the STAs are not evenly distributed around the GCS (see Fig. 5), the aggregate throughput at the F-AP for the static strategy decreases rapidly as the STAs move farther away. Compared to the static strategy, dynamic strategies offer huge improvements for this mobility model, as shown in Table II. The static and MAT-G strategies offer the same aggregate throughput at the AP and at the GCS, so aggregate throughput at the GCS (dashed lines) is not visible for these strategies in Fig. 8. This proves that for both of these strategies the

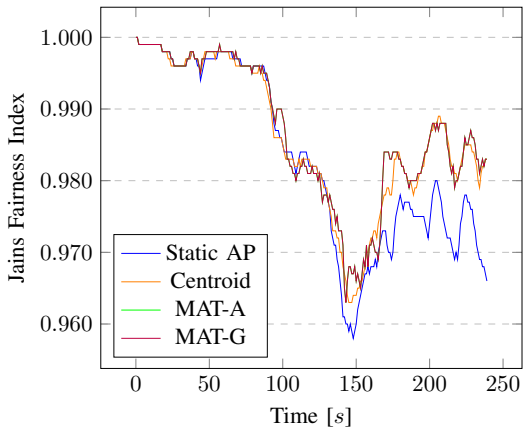


Fig. 7. Jain's Fairness Index for each F-AP positioning strategy in a scenario where STAs follow mobility pattern 1.

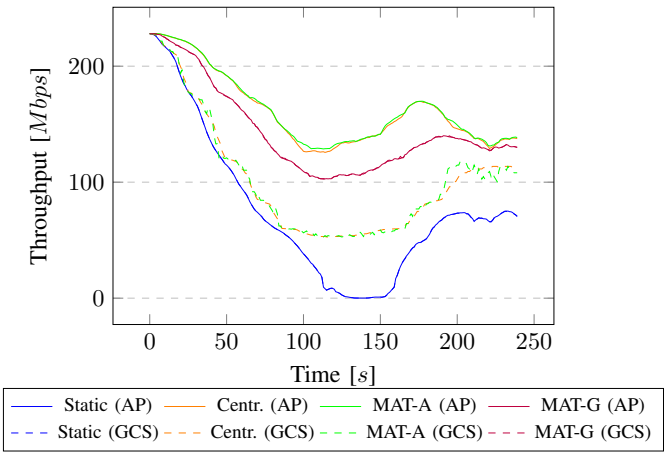


Fig. 8. Aggregated throughput to F-AP (solid line) and GCS (dashed line) for each F-AP positioning strategy in a scenario where STAs follow mobility pattern 2.

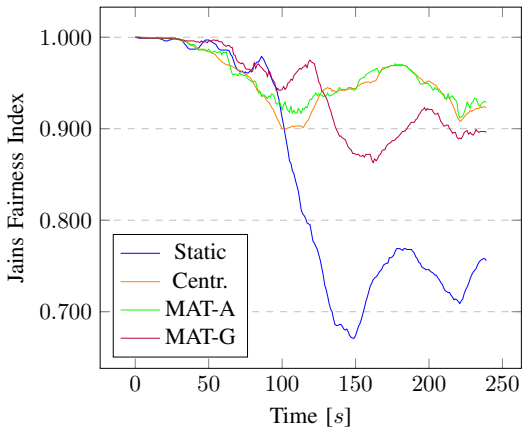


Fig. 9. Jain's Fairness Index for each F-AP positioning strategy in a scenario where STAs follow mobility pattern 2.

most restrictive capacity is that of the access network (i.e., aggregate throughput at the F-AP). Between seconds 129 and 151, the aggregate throughput at the F-AP for the static strategy falls below 1 Mbps, reaching the bottom with 71 kbps at second 138. At the same time, Jain's fairness index falls below 0.7. We use Jain's index to quantify capacity fairness among STAs, with 1 indicating equal throughput for all STAs. The MAT-G strategy also experiences a faster reduction in the aggregate throughput at the F-AP compared to the other dynamic strategies; however, it maintains a more favorable performance for aggregate throughput to GCS. The centroid and MAT-A strategies are the only strategies in which the backhaul link becomes the bottleneck in the network architecture. Consequently, aggregate throughput at the GCS differs from that at the F-AP (Fig. 8). Comparing centroid and MAT-A strategies reveals no substantial differences, except a slight MAT-A advantage in Jain's Fairness Index (Fig. 9) and minor backhaul variations late in the evaluation, when STAs disperse across the scenario. These discrepancies stem from MAT-A accounting for the non-linear distance-throughput relationship in empirical measurements. Since in empirical measurements MCS changes cause discrete throughput gaps, while stable regions occur when a given MCS is maintained.

3) Mobility model 3: In this case, the STAs are positioned in an aligned formation along one side of the square at the beginning. The inter-node spacing is 2 meters. Both GCS and F-AP are located at the center of the area (Tab. I). The STAs then travel from their initial side of the square to the opposite one. This type of movement emulates the behavior of a squad performing a line sweep search, for example. Once the line of STAs reaches the opposite side, they turn around and return along the same path.

The main difference between this mobility model and the others is that the STAs are contained in a reduced area and move uniformly in a deterministic way (Fig. 5). Since relative positions between STAs remain static, centroid and MAT-A strategies achieve a stable aggregate throughput at the F-AP (Fig. 10). For the same strategies, the aggregate throughput to GCS increases and decreases as the distance between F-AP and GCS shrinks and grows, respectively (Fig. 10). The MAT-G strategy obtains good performance for all KPIs. Although the centroid and MAT-A strategies outperform it in terms of aggregate throughput at the F-AP (Fig. 10), the results in relation to the aggregate throughput to the GCS compensate for this disadvantage, as shown by the improvement percentages in Table II. Regarding Jain's Fairness Index, all strategies report good performance thanks to the proximity of the STAs to each other (Fig. 11).

C. Energy and computational costs

Beyond throughput and fairness, energy consumption is a key aspect of F-AP placement, as UAV operations are limited by autonomy. This section analyzes the proposed strategies from this perspective, considering displacement consumption.

Although the optimization-based strategy here relies on ES for evaluation, the optimal solution can still be computed in practical time for certain network sizes and spatial resolutions. The section therefore also studies its computational complexity

TABLE II
COMPARATIVE STRATEGY AVERAGE AGGREGATE THROUGHPUT PERFORMANCE ACROSS MOBILITY MODELS. PARENTHESES INDICATE PERCENTAGE IMPROVEMENT OVER STATIC AP STRATEGY.

	Mobility Model 1				Mobility Model 2				Mobility Model 3			
	To AP		To GCS		To AP		To GCS		To AP		To GCS	
	Mbps	(%)	Mbps	(%)	Mbps	(%)	Mbps	(%)	Mbps	(%)	Mbps	(%)
centroid	199	(1)	199	(1)	171	(180)	96	(58)	223	(88)	121	(2)
MAT-A	200	(1)	200	(1)	172	(182)	97	(59)	223	(88)	123	(4)
MAT-G	200	(1)	200	(1)	144	(137)	144	(137)	183	(55)	183	(55)
static_ap	198	(0)	198	(0)	61	(0)	61	(0)	119	(0)	119	(0)

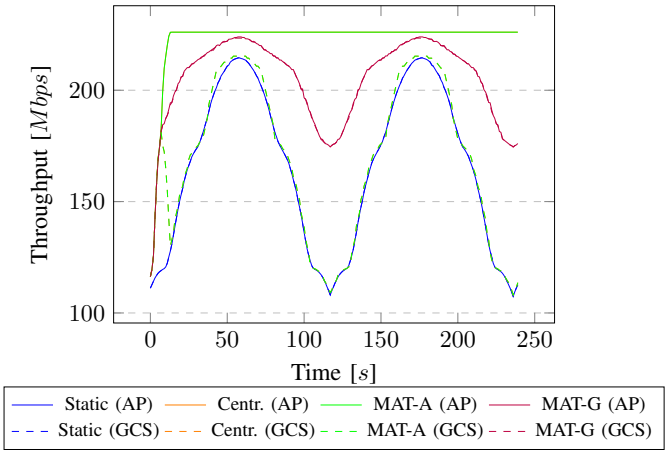


Fig. 10. Aggregated throughput to F-AP (solid line) and GCS (dashed line) for each F-AP positioning strategy in a scenario where STAs follow mobility pattern 3.

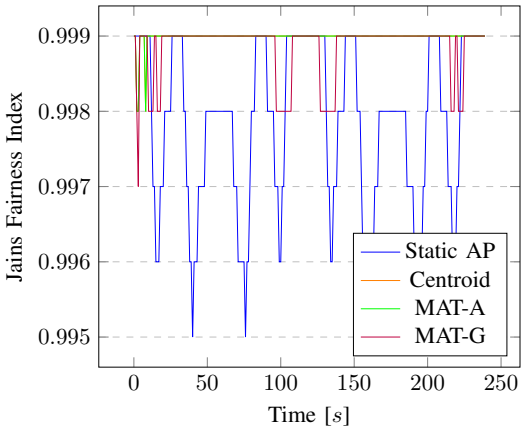


Fig. 11. Jain's Fairness Index for each F-AP positioning strategy in a scenario where STAs follow mobility pattern 3.

and the resulting implications for the achievable F-AP position update rate.

1) Energy consumption: To estimate the consumption of the UAV, only the energy used to accelerate the UAV and the energy consumption resulting from drag are considered. This estimation does not include the energy employed to maintain the UAV in the air since that component is the same for all approaches. Therefore, the energy consumption follows Eq. 3.

$$E = W_T + W_D \tag{3}$$

Where W_T is the consumption resulting from the thrust needed to accelerate the UAV and W_D is the work needed to counter the drag. This consumption analysis is performed taking the DJI Phantom UAV as reference. This choice is based on the work presented in [18] and [19], where the authors characterize the drag associated with this UAV model. W_{T_i} is calculated using Eq. 4.

$$W_T = \sum_{i=0}^{T} \vec{F}_i \cdot \vec{d}_i = m \sum_{i=1}^{T} \vec{a}_i \cdot \vec{d}_i \tag{4}$$

The acceleration $\vec{a}_i$ and the distance $\vec{d}_i$ for each time frame i are obtained from the position traces.

W_D represents the work that the rotors have to spend to generate the needed thrust to compensate the drag when the UAV is moving. Eq. 5 shows how this value is calculated.

$$W_D = \sum_{i=0}^{T} \vec{F}_{D_i} \cdot \vec{d}_i \tag{5}$$

$\vec{F}_{D_i}$ is the drag, and its calculation is based on aerodynamic principles. At velocities lower than $10\,m/s$, drag can be approximated as a linear function depending on the velocity [18]. Since the maximum velocity considered in the scenario is 5 m/s, the drag $\vec{F}_{D_i}$ is calculated as:

$$\vec{F}_{D_i} = \rho \cdot K_i \cdot \vec{V}_i \tag{6}$$

K_i is a coefficient that encloses the particularities of the body in movement, such as the shape, angle of incidence of air, surface material, rotor velocity, etc. As an approximation, the rotors are considered to spin at a constant velocity of 5300 RPM, which is the velocity the DJI Phantom UAV needs to hover [19]. The following model is obtained from [18] to calculate the value of the coefficient K, considering that the angle of attack α does not exceed 10 degrees. Please refer to [18] for further details on the computation of α, which is equal to 9° for the considered maximum speed of 5 m/s.

$$K_i = 0.295 - 0.0045 \cdot \alpha \tag{7}$$

Fig. 12 shows the total consumption of the three dynamic strategies for the three proposed mobility models. It demonstrates that optimization-based strategies are significantly more

energy-intensive than geometry-based strategies for mobility patterns 1 and 2. In this context, the stability of the centroid position offers a distinct advantage over the variability of the maximums detected by the ES algorithm. The instability of the best position in optimization-based strategies causes the UAVs to change directions frequently, which entails higher energy consumption. Regarding mobility pattern 3, MAT-A and centroid strategies yield similar results because the relative positions between STAs remain unchanged. Conversely, the MAT-G strategy consumes more energy as it necessitates frequent repositioning maneuvers toward and from the GCS to balance access and backhaul capacities. The power consumption of a DJI Phantom in hovering mode is approximately 250 W [20]. Considering this value, the energy savings yielded by the centroid approach, relative to the MAT-A approach, are approximately 6% for mobility pattern 1. For mobility pattern 2, the efficiency improvement is between 4 % and 5%. Finally, simulations reveal that increasing the number of STAs marginally improves the energy efficiency of the centroid strategy under mobility patterns 1 and 2. The consumption is reduced by around 0.7 $W \cdot min$ when scaling from 5 to 15 STAs. This occurs because a larger sample size mitigates the impact of individual node stochasticity, yielding a more stable F-AP trajectory. In contrast, optimization-based strategies exhibit negligible fluctuations in power consumption relative to STA density.

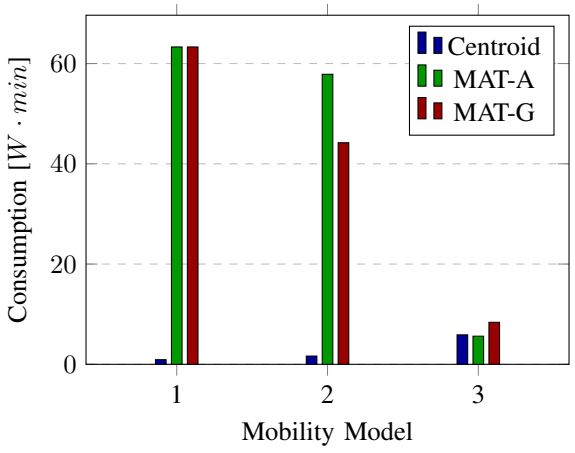


Fig. 12. Consumption resulting from displacement.

2) Computational costs: This section analyzes the computational cost of the ES used to implement the optimization-oriented F-AP placement strategy. Although this approach provides an optimal reference for the evaluated KPIs, practical deployments may rely on lower-complexity heuristics that approximate this solution with limited performance loss. The algorithm's time complexity is inherently constrained by the spatial grid size, G, and the number of STAs, U. Specifically, calculating the link quality for all U users across every candidate position results in an overall complexity of $O(G \cdot U)$. The configuration used for previous analysis consists of fixing the grid resolution r to 1 m. It is intentionally detailed to support our comparative analysis of the proposed strategies. However, it is unnecessarily demanding for practical deployment, with execution times of 3-13 minutes per snapshot for 5–15 STAs on a mid-range desktop PC (i7-13700@2.1 GHz CPU). Fig. 13 illustrates the calculation time (in seconds, on a logarithmic scale) required by the ES algorithm as a function of the spatial resolution interval (x-axis) and the number of STAs. As observed, the computational cost is heavily dominated by the spatial grid resolution. Reducing the resolution interval from 10 m to 1 m leads to an execution time increase of two orders of magnitude from an average of $\sim 5s$ to $\sim 500s$. This empirically confirms the inversely quadratic complexity, $O(\frac{1}{r^2})$, with respect to the grid step size. Furthermore, within a fixed resolution, increasing STAs from 5 to 15 proportionally increases calculation time, validating the $O(U)$ linear complexity regarding users at each position. Fig. 13 also plots the average aggregate throughput at the F-AP for different intervals. The plotted values are relative to the results for the $1m$ interval, and only the MAT-A strategy was considered. ES remains feasible for moderate networks, particularly for 5–15 STAs and grid resolutions of a few meters (i.e., from $5m$ onward). For practical implementation, the resolution can be set to $10m$. With this modification, computation times fall below 5 seconds, while the performance drop does not reach 0.5 %. This would provide a reasonable updating rate for the F-AP position, without sacrificing near-optimal performance. More efficient heuristics, which we are currently developing, can further decrease the computational cost.

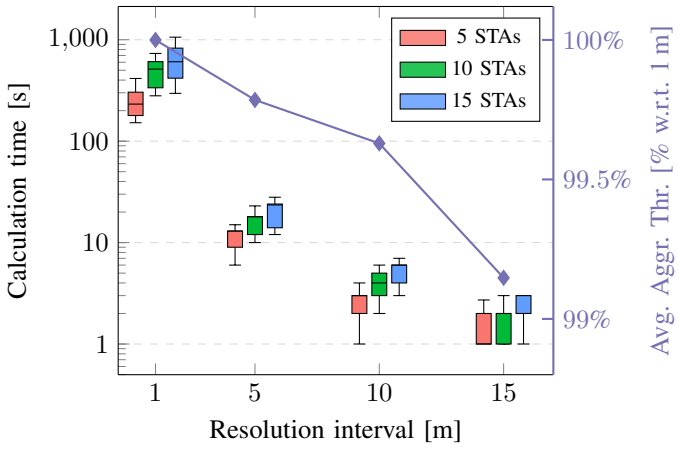


Fig. 13. Calculation time (left axis) and average relative aggregate throughput at the F-AP with respect to 1 m (right axis) per resolution interval.

V. Conclusions and Future Work

In this paper, an analysis of several strategies for the deployment of an F-AP is presented. The strategies have been tested for scenarios where STAs move following different mobility models. The results demonstrate that leaving the AP at a fixed point is suitable when the STAs are uniformly distributed around both the AP and the GCS. In such scenarios, it provides stable performance without requiring repositioning mechanisms. Conversely, the MAT-G strategy proves to be highly

advantageous when the STAs are concentrated within a limited area and tend to move far from the GCS. Giving a situation analogous to cluster-based mobility patterns. MAT-A strategy offers a more realistic representation of network performance since it captures the discrete steps in the throughput–distance curve caused by changes in the MCS successfully. However, its overall impact remains limited compared to positioning the F-AP at the centroid. Consequently, the centroid-based strategy achieves performance comparable to the MAT-A approach while being considerably more efficient from a computational perspective. Also note that the considered simplifications, such as LoS, absence of hidden nodes, and throughput mapping from distance, make geometry-based approaches more competitive. However, optimization-based approaches would take advantage in more complex scenarios.

As future work, we consider employing more realistic mobility models. Reducing ES-based strategies' computation costs by means of heuristics is crucial, since they become excessively complex when the number of STAs or scenario size increases. Search and rescue is an interesting use case to apply the mechanisms presented in this paper. Applying them to scenarios with mobility models such as those present in search and rescue operations would be useful to perform a more realistic evaluation. Also, the exploration of new mechanisms to optimize the F-AP positioning based on Machine Learning (ML) methodologies, enabling the resolution of more complex scenarios such as urban or hilly ones, is a feasible and interesting line of research for future work.

Acknowledgment

This research was funded in part by the Spanish MCIN/AEI/10.13039/501100011033/FEDER/UE through project PID2023-146378NB-I00. It also has the support of the FI-STEP (2025 STEP 00109) from the Department of Research and Universities of the Generalitat de Catalunya and the co-financing of the European Social Fund Plus(FSE+).

References

[1] F. Avishan et al. "Optimization of drone base station locations and mobile charging drone routing for post-disaster communication". In: *Computers & Operations Research* 184 (Dec. 2025), p. 107206.

[2] Y. Qin, M. A. Kishk, and M.-S. Alouini. "Drone Charging Stations Deployment in Rural Areas for Better Wireless Coverage: Challenges and Solutions". In: *IEEE Internet of Things Magazine* 5.1 (Mar. 2022), pp. 148–153.

[3] B. Kirubakaran and J. Hosek. "Optimizing Tethered UAV Deployment for On-Demand Connectivity in Disaster Scenarios". In: 2023 IEEE 97th Vehicular Technology Conference (VTC2023-Spring). Florence, Italy: IEEE, June 2023, pp. 1–6.

[4] M. N. Marques et al. "Tethered Unmanned Aerial Vehicles—A Systematic Review". In: *Robotics* 12.4 (Aug. 14, 2023), p. 117.

[5] Y. Sun et al. "3D hybrid TOA-AOA source localization using an active and a passive station". In: 2016 IEEE 13th International Conference on Signal Processing (ICSP). Chengdu, China: IEEE, Nov. 2016, pp. 257–260.

[6] N. Salman, M. W. Khan, and A. H. Kemp. "Enhanced hybrid positioning in wireless networks II: AoA-RSS". In: 2014 International Conference on Telecommunications and Multimedia (TEMU). Heraklion, Crete, Greece: IEEE, July 2014, pp. 92–97.

[7] H.D. Sherali, C.M. Pendyala, and T.S. Rappaport. "Optimal location of transmitters for micro-cellular radio communication system design". In: *IEEE Journal on Selected Areas in Communications* 14.4 (1996), pp. 662–673. DOI: 10.1109/49.490417.

[8] Onur Tekdas, Wei Yang, and Volkan Isler. "Robotic Routers: Algorithms and Implementation". In: *The International Journal of Robotics Research* 29.1 (2010), pp. 110–126. DOI: 10.1177/0278364909105053. eprint: https://doi.org/10.1177/0278364909105053. URL: https://doi.org/10.1177/0278364909105053.

[9] E. Nakata, T. Ebihara, and K. Mizutani. "Mobile robotic access point for transitional optimization of wireless access point positioning". In: 2014 IEEE 3rd Global Conference on Consumer Electronics (GCCE). Tokyo, Japan: IEEE, Oct. 2014, pp. 439–441.

[10] Akram Al-Hourani, Sithamparanathan Kandeepan, and Simon Lardner. "Optimal LAP Altitude for Maximum Coverage". In: *IEEE Wireless Communications Letters* 3.6 (2014), pp. 569–572. DOI: 10.1109/LWC.2014.2342736.

[11] Mohammad Mozaffari et al. "Efficient Deployment of Multiple Unmanned Aerial Vehicles for Optimal Wireless Coverage". In: *IEEE Communications Letters* 20.8 (Aug. 2016), pp. 1647–1650. arXiv: 1606.01962[cs].

[12] X. Zhong et al. "Joint Optimization of Relay Deployment, Channel Allocation, and Relay Assignment for UAVs-Aided D2D Networks". In: *IEEE/ACM Transactions on Networking* 28.2 (Apr. 2020), pp. 804–817.

[13] G. Santos et al. *A Fast Gateway Placement Algorithm for Flying Networks*. Mar. 8, 2021. DOI: 10.48550/arXiv.2010.06732. arXiv: 2010.06732[cs].

[14] G. Papanikolaou-Ntais et al. "Optimizing Access Point Placement Using Gnn for Enhancing Indoors Ue Localization". In: 2025 Joint European Conference on Networks and Communications & 6G Summit (EuCNC/6G Summit). Poznan, Poland: IEEE, June 3, 2025, pp. 817–822.

[15] V. Mayor et al. "Deploying a Reliable UAV-Aided Communication Service in Disaster Areas". In: *Wireless Communications and Mobile Computing* 2019 (Apr. 8, 2019), pp. 1–20.

[16] E. Garcia et al. "Achievable Bandwidth Estimation for Stations in Multi-Rate IEEE 802.11 WLAN Cells". In: 2007 IEEE International Symposium on a World of Wireless, Mobile and Multimedia Networks. Espoo, Finland: IEEE, June 2007, pp. 1–8.

[17] G. Betcher-Sbrolla, E. Lopez-Aguilera, and E. Garcia-Villegas. "Analysis and Proposal of Strategies for the Management of Drone Swarms Through Wi-Fi Technologies". In: *Drones* 9.8 (Aug. 18, 2025), p. 584.

[18] K. Meier et al. "Wind Estimation with Multirotor UAVs". In: *Atmosphere* 13.4 (Mar. 29, 2022), p. 551.

[19] C. Russell et al. "Wind Tunnel and Hover Performance Test Results for Multicopter UAS Vehicles". In: Vertical Flight Society 72nd Annual Forum and Technology Display. West Palm Beach, Florida: The Vertical Flight Society, May 17, 2016, pp. 1–20.

[20] Nigel. *Drone Power and Energy Estimation*. Battery Design. Jan. 12, 2026. URL: https://www.batterydesign.net/drone-power-and-energy-estimation/.